Archive of Applied Mechanics (2022) 92:3999–4015
https://doi.org/10.1007/s00419-022-02277-0

ORIGINAL

**Yuan Zhang · Lei Zhang · Sigong Zhang**

# Exact series solutions of composite beams with rotationally restrained boundary conditions: static analysis

Received: 19 February 2022 / Accepted: 25 September 2022 / Published online: 8 October 2022


**Abstract** The structural performance of composite beams is sensitive to load distribution as well as actual boundary conditions. Although the composite beam theory has been solidly established and exact solutions have been readily developed for various loading and boundary conditions, almost all of them are limited to classical boundary conditions (free, pinned and clamped) and there has been little discussion about the actual support conditions in real structures. The general representation of actual boundary conditions can be defined as rotationally restrained edges. In this research, an analytical model with exact series-type solutions was developed for composite beams with rotationally restrained edges. The model and displacement solutions were validated by other analytical methods and numerical results. The influence of rotational and end-slip restraints was investigated. It was found that the deflection and interface slip of composite beams are highly affected by both restraints introduced by the actual boundary conditions. The current model can be used as a benchmark for future design methods considering the realistic boundary conditions of composite beams.

**Keywords** Partial composite action · Gamma method · Stokes' transformation · Fourier series · End fixity factors · End-slip restraints

## 1 Introduction

Composite structures combining dissimilar materials through various shear connectors are extensively implemented in civil engineering applications as floor/wall components and bridge decks. The most common form of composite elements in construction is steel–concrete composites, which has attracted tremendous research interests over last decades (e.g. [1–3]). In parallel, other types of composites including steel–timber and timber–concrete composites (TCC) have been increasingly developed as alternative solutions to traditional reinforced concrete and steel–concrete composites or refurbishment techniques for existing structures. More recently, with rapidly emerging movement towards sustainable construction and significant advances in engineered wood products and mass timber panels, TCC systems have been increasingly used in new structures and present numerous advantages over timber-only or reinforced concrete floors [4,5]. Such a trend substantially fuels the need to improve the existing analysis procedure and design methods for composite beams.

Y. Zhang
College of Architecture and Transportation, Liaoning Technical University, Fuxin 123000, Liaoning, China

L. Zhang
Department of Civil and Environmental Engineering, University of Alberta, Edmonton, AB T6G 2R3, Canada

S. Zhang (✉)
School of Engineering, Newcastle University, Newcastle upon Tyne NE1 7RU, UK
E-mail: sigong.zhang@newcastle.ac.uk

The behaviour of composite members is complex as the shear connectors generally permit relative slip between individual components of the member and only partial composite action can be achieved [6]. Since 1940s, a considerable amount of literature has been published on the composite beam theory from linear elastic models [7–11] to nonlinear plastic methods [12–15]. A detailed background to the composite beam theory and the literature in the field can be found in [16]. Based on earlier theoretical models, simplified design methods for composite beams with partial interaction have been developed. In timber engineering, simplified design approaches such as Gamma method in Eurocode 5 (Annex B) [17] and Newmark–McCutcheon formula [8,18,19] have been commonly used in practical designs. The Gamma method, which was recommended by Ceccotti [4] for linear-elastic analysis, was developed based on the simple linear elastic model of Möhler [9] for timber–timber composite beams and derived from the exact solution for a simply supported composite beam subjected to a sinusoidal distributed load. A closely related deduction can be found in [20]. According to this approach, the "Effective Stiffness" concept is introduced and a "Connection Efficiency Factor" ($\gamma$) is used to account for the composite efficiency of shear connectors, with $\gamma = 1$ representing fully composite action, and $\gamma = 0$ no connection at all. It also provides an elegant solution with acceptable accuracy for simply supported beams under a uniformly distributed load or concentrated load. In addition, the coefficient of $\gamma$ renders a favourable illustration of the nature of the problem [21]. In parallel, Newmark et al. [8] developed similar elastic composite beam model for steel–concrete composite beams and derived the exact solution for simply supported composite beam under a concentrated load. The expression was simplified by McCutcheon [18,19] for timber components, which is denoted as Newmark–McCutcheon formula herein. Surprisingly, these two independent methods (Gamma method and Newmark–McCutcheon formula) produced almost the same result. The Newmark–McCutcheon formula has been widely used in North America for calculating effective composite bending stiffness such as ATC Design Guide 1 [22].

However, increasing concerns have been raised about the validity and accuracy of the well-known simplified methods for arbitrary boundary conditions other than the simple support. Exact solutions and simplified formula have been readily developed on various boundary conditions for uniform composite beams [6,11,16,23–25]. It has been found that the error of the Gamma method in the clamped–clamped case is around 20% [25], even up to almost 30% [16]. For extensions of the Gamma method to beams with other boundary conditions, Eurocode 5 [17] recommends 0.8 of the relevant span for continuous beams and twice the length for cantilever beams. Furthermore, a general and more accurate way of determining the effective beam length was proposed by Girhammber [16] for arbitrary boundary and loading conditions.

The newly proposed design methods/formulas for so-called arbitrary boundary conditions [16,23] merely cover an arbitrary combination of free, pinned (simply supported) and clamped conditions. These conditions are idealized extreme conditions that do not reflect actual boundary conditions in structures. In fact, it is prohibitively difficult, if not impossible, to achieve clamped conditions, such that all displacement and rotation components vanish, at supports [26], especially for timber since it is relatively 'compressible' in the across grain direction [27]. In most simply supported cases, some amount of rotational stiffness can be introduced by the boundary conditions. For instance, platform-frame construction in timber engineering often result in large restraints at end supports due to weight of upper stories [28]. In reality, the boundary conditions are normally semi-rigid, which can be defined as restrained conditions against rotation. Nevertheless, very little attention has been paid to the actual support conditions for composite beams.

The current research aims to fill this gap by developing an analytical model for static analysis of composite beams with rotationally restrained edges and deriving an exact series solution. Series type solutions (e.g. Navier solution and Levy solution) have been extensively used for simple beam and plate structures from the beginning of the last century [29] and have also been applied to composite beams [30], stressed-skin panels [31] and stiffened plates [32]. The benefit of series-type solutions is that they can be easily generalized for various loading scenarios and boundary conditions. While the application of series type solutions is straightforward to various loading cases, it turns out to be rather tedious to satisfy complex boundary conditions. Accordingly, rigorous series-type solutions are widely applied for simply supported conditions. Although laborious superposition techniques can be used [33] for complex boundary conditions, it is common practice to resort to approximate techniques based on Ritz–Galerkin methodology or direct numerical analysis [34]. It is the use of Stokes' transformation that releases those complex boundary conditions [35] leading to a simple, unified and systematic procedure dealing with beams and plates with arbitrary boundary conditions [36–38].

In the current study, the series-type solutions with the employment of Stokes' transformation were extended to composite beams with rotationally restrained edges. The fourth-order governing differential equations for the displacement of partially composite beams with rotationally restrained edges were first derived. Then, by applying Stokes' transformation, exact series solutions were deducted. The validity and accuracy of the

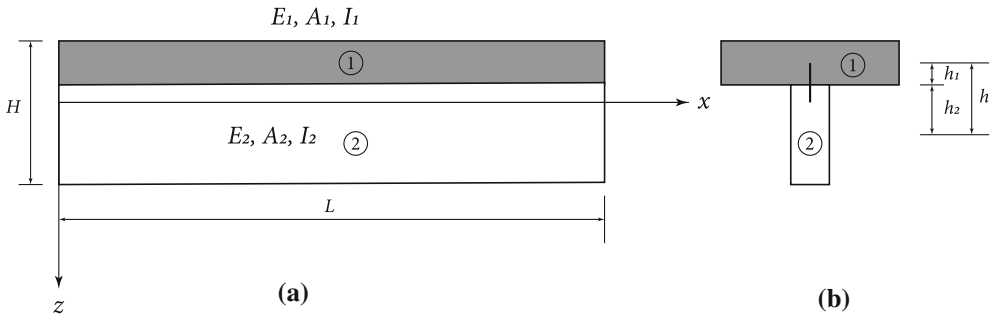


**Fig. 1** A typical composite beam and the coordinate system: **a** elevation; **b** cross section

proposed solution were assessed by comparing predicted deflections and slips with other analytical models and numerical results. Finally, the parametric studies were conducted to examine the influence of different boundary restraints.

## 2 Formulation

### 2.1 Governing equations

The present model is based on Euler–Bernoulli beam theory (for each element of the composite beam). All materials (including shear connectors) are assumed to remain within the linear-elastic range until elements fail. The shear connectors between two elements are regarded as continuous and uniformly distributed along the longitudinal direction. Elements are subjects to bending and no axial loads are applied.

A typical composite beam with two sub-elements of different materials, as shown in Fig. 1, is studied. $E_i$, $A_i$ and $I_i$ ($i = 1,\ 2$) are Young's modulus, cross-sectional area and moment of inertia of two elements. $L$ and $H$ denote the length and height of the composite beam, respectively. The symbol $h_1$ denotes the distance from the centroid of the upper element to the interface between the elements. Similarly, the distance from the centroid of the lower element to the interface is represented by $h_2$. The subscripts "1" and "2" will refer to the upper and lower elements, respectively. The $x$-axis of the coordinate system is located in the centroid of the composite section. The coordinate origin is placed at the left support, and the positive direction of $z$-axis is downward. The displacements in the $x$- and $z$-directions are denoted as $u$ and $w$, respectively.

The kinematical relation can be determined first. In the case that partial composite action is developed between two elements, the interface slippage presents. Based on the above assumptions, the geometrical relation of the slippage $u_\mathrm{s}$, the deflection $w$ and the axial displacements of two components, $u_1$ and $u_2$, is illustrated in Fig. 2. Thus, the relation between the slippage $u_\mathrm{s}$ and the deflection $w$ is

$$u_\mathrm{s} = u_2 - u_1 + w'h \tag{1}$$

Then, equilibrium of forces can be established. Fig. 3 shows a free-body diagram of an infinitesimal element of length d$x$ with internal and external forces upon it. Bending moment, shear force and axial force are denoted by $M$, $Q$ and $N$, respectively. Equilibrium equations for the element are

$$Q' = -q \tag{2a}$$
$$N_1 + N_2 = 0 \tag{2b}$$
$$M' = Q \tag{2c}$$

Considering the equivalence of the internal and external actions on the left-hand side of the free-body diagram in Fig. 3, it can be obtained

$$Q = Q_1 + Q_2 \tag{3a}$$
$$N_1' = -N_2' = -q_\mathrm{s} \tag{3b}$$
$$M = M_1 + M_2 - N_1 h \tag{3c}$$

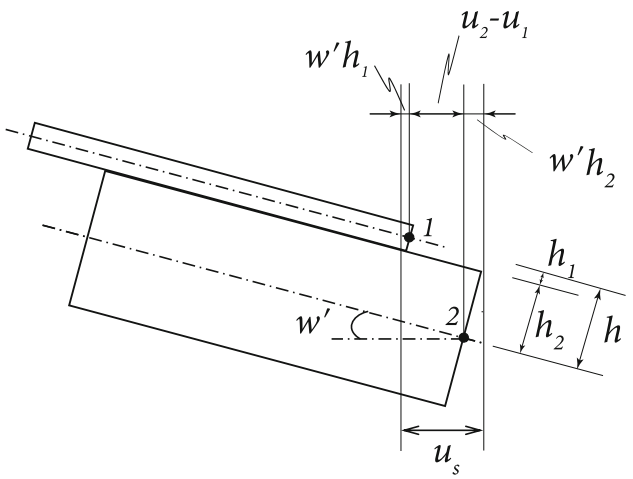


**Fig. 2** Kinematic relation between interlayer slip and axial and transverse displacements (adopted from [39])

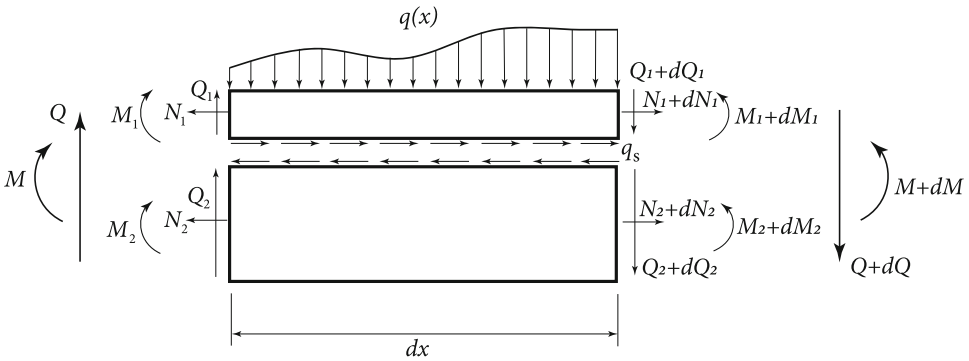


**Fig. 3** An infinitesimal element of the composite beam

Assuming both layers have equal curvature, it yields

$$\frac{M_1}{E_1 I_1} = \frac{M_2}{E_2 I_2} = -w'' \tag{4}$$

Thus, the internal axial forces can be expressed with the first derivative of displacements as:

$$N_1 = E_1 A_1 u_1', \quad N_2 = E_2 A_2 u_2' \tag{5}$$

The first governing equation can be obtained by combining Eqs. (2b) and (5) as:

$$E_1 A_1 u_1' + E_2 A_2 u_2' = 0 \tag{6}$$

The relation of the interface slippage and the shear force of the shear connector is

$$q_6 = k u_s \tag{7}$$

where $k$ denotes the shear stiffness of the shear connector per unit length (unit: $\mathrm{N/m^2}$). Applying Eq. (3b), it gives

$$N_1' = -N_2' = -k u_s \tag{8}$$

By considering Eqs. (1), (5) and (8), the second governing equation can be derived as:

$$E_1 A_1 u_1'' + k(u_2 - u_1 + h w') = 0 \quad \text{or} \quad E_2 A_2 u_2'' - k(u_2 - u_1 + h w') = 0 \tag{9}$$

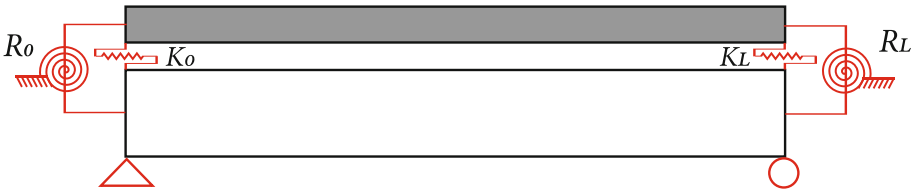


**Fig. 4** General boundary conditions (shear connectors are not shown here for clarity)

Finally, substituting Eqs. (4) and (5) in Eq. (3c) results in

$$M = -EI_o w'' - E_1 A_1 h u_1' \tag{10}$$

where $EI_o = E_1 I_1 + E_2 I_2$. Then, substituting Eqs. (2c), (10) in (2a), it gives

$$EI_o w'''' + E_1 A_1 h u_1''' = q \tag{11}$$

which is the third governing differential equation.

## 2.2 General boundary conditions

In order to simulate different boundary conditions, two types of springs were defined to characterize all possible intermediate end supports of a single-span composite beam from simply supported to fully clamped as shown in Fig. 4. Two external springs represent the rotational restraints, $R_0$ and $R_\mathrm{L}$, and two internal springs restrain the slip at the beam ends, $K_0$ and $K_\mathrm{L}$, denoted as end slip restraints herein (or end shear restraints in [40–42]). The rigid end-slip restraint was found to have a significant effect on the behaviour of composite beams, especially when the intermediate shear connector stiffness between two members of a composite beam is small [42]. However, very little attention has been paid to the role of the end slip restraint in the existing composite beam theories.

Rigid shear restraints were defined in [40] to suppress the shear deformation at beam ends leading to plane section at composite beam ends as shown in Fig. 5b, which can be realized by a special support design (although quite rare in current practice). Numerical results [41] have shown that rigid shear restraints exert a stiffening action to the beam and significantly reduce the displacement [42]. In this study, a more general end-slip restraint was defined to characterize a broad range of slip conditions at the beam ends. For zero end-slip restraints, each member of a composite beam freely elongates leading to larger slip at beam ends. Similarly, infinite end-slip restraints imposes the end sections to remain plane (no slip), which was defined as rigid shear restraints in [40]. In addition, although the end-slip restraints are introduced together with the rotational restraints, they can be considered separately. That means even for simply supported beam (with free rotations at the beam ends), end-slip restraints can be added to improve the composite actions.

Six boundary conditions are required to solve the system of governing equations. The general boundary conditions (Fig. 4) can be expressed as:

$$w(0) = w(L) = 0 \tag{12a}$$

$$M(0) = R_0 w'(0), \quad M(L) = -R_\mathrm{L} w'(L) \tag{12b}$$

$$u_\mathrm{s}(0) = -N_1(0)/K_0, \quad u_\mathrm{s}(L) = N_1(L)/K_\mathrm{L} \tag{12c}$$

It should be noted that $u_\mathrm{s}(0)$ is negative because the element 1 moves in the negative $x$-direction and undergoes negative displacement. Substituting Eq. (8) in Eq. (12c) gives

$$N_1'(0)/k = N_1(0)/K_0, \quad -N_1'(L)/k = N_1(L)/K_\mathrm{L} \tag{13}$$

Substituting Eqs. (10) and (5) in Eqs. (12b) and (13), respectively, the boundary conditions can be expressed in the form of displacement, rotation, and slip as:

$$w(0) = w(L) = 0 \tag{14a}$$

$$EI_o w''(0) + E_1 A_1 h u_1'(0) = R_0 w'(0), \quad EI_o w''(L) + E_1 A_1 h u_1'(L) = -R_\mathrm{L} w'(L) \tag{14b}$$

$$u_1'(0) = \frac{K_0}{k} u_1''(0), \quad u_1'(L) = -\frac{K_\mathrm{L}}{k} u_1''(L) \tag{14c}$$

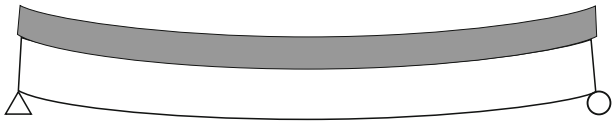

**(a)** Without end shear restraints

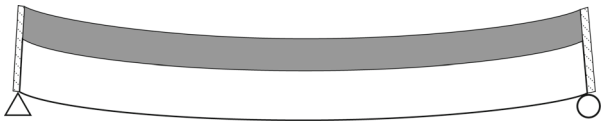

**(b)** End shear restraints

**Fig. 5** End conditions of elastic composite beam with/without end shear restraint (after [40])

## 3 Exact series solution

The displacement functions can be expressed as Fourier series of the form:

$$w(x) = \sum_{m=1}^{\infty} A_m \sin \alpha_m x, \quad 0 \leqslant x \leqslant L \tag{15}$$

$$u_1(x) = B_0 + \sum_{m=1}^{\infty} B_m \cos \alpha_m x, \quad 0 \leqslant x \leqslant L \tag{16}$$

$$u_2(x) = C_0 + \sum_{m=1}^{\infty} C_m \cos \alpha_m x, \quad 0 \leqslant x \leqslant L \tag{17}$$

where $\alpha_m = m\pi/L$ and $A_m$, $B_m$ and $C_m$ are the Fourier coefficients. In general, the applied load can be given by

$$q(x) = \sum_{m=1}^{\infty} Q_m \sin \alpha_m x, \quad 0 \leqslant x \leqslant L \tag{18}$$

where

$$Q_m = \frac{2}{L} \int_0^L q(x) \sin \alpha_m x \mathrm{d}x \tag{19}$$

With a given external force $q(x)$, these Fourier coefficients can be determined by substituting the displacement functions [Eqs. (15), (16) and (17)] in the governing differential equations of Eqs. (6), (9) and (11). The derivation process is presented as follows.

In particular, the derivative of the displacement functions must be carefully handled because term-by-term differentiation may not be valid. A special differentiation technique called Stokes' transformation can be applied. Mathematical discussions and proofs on this topic can be found on pages 137–139 in [43] and on pages 375–377 in [44]. The first to fourth derivatives of Fourier sine series and cosine series can be found in [36,45].

Based on Stokes' transformation, the first derivative of $w(x)$ can be expressed as:

$$w'(x) = \sum_{m=1}^{\infty} \alpha_m A_m \cos \alpha_m x, \quad 0 \leqslant x \leqslant L \tag{20}$$

However, with regard to the first derivative of $u_1$ and $u_2$, term-by-term differentiation is only valid on open interval of $0 < x < L$. They can be expressed as:

$$u_1' = -\sum_{m=1}^{\infty} \alpha_m B_m \sin \alpha_m x \tag{21}$$

$$u_2' = -\sum_{m=1}^{\infty} \alpha_m C_m \sin \alpha_m x \tag{22}$$

Substituting Eqs. (21) and (22) in Eq. (6), the first governing equation can be expressed as:

$$\sum_{m=1}^{\infty} \alpha_m (E_1 A_1 B_m + E_2 A_2 C_m) \sin \alpha_m x = 0 \tag{23}$$

Since Eq. (23) is valid for any $x$ (or Cantor's theorem [46]), it can be concluded that

$$E_1 A_1 B_m + E_2 A_2 C_m = 0 \tag{24}$$

The second derivative of $u_1$ on interval of $0 \leqslant x \leqslant L$ can be obtained as:

$$u_1'' = \frac{u_1'(L) - u_1'(0)}{L} + \sum_{m=1}^{\infty} \left\{ \frac{2}{L}\left[(-1)^m u_1'(L) - u_1'(0)\right] - \alpha_m^2 B_m \right\} \cos \alpha_m x \tag{25}$$

Substituting Eqs. (16), (17), (20) and (25) in the second governing equation of Eq. (9), it gives

$$\begin{aligned} &\frac{E_1 A_1}{k}\left[u_1'(L) - u_1'(0)\right] + k(C_0 - B_0) + \sum_{m=1}^{\infty} \left\{ \frac{2E_1 A_1}{L}\left[(-1)^m u_1'(L) - u_1'(0)\right] - E_1 A_1 \alpha_m^2 B_m \right. \\ &\left. + k(C_m - B_m) + kh\alpha_m A_m \right\} \cos \alpha_m x = 0 \end{aligned} \tag{26}$$

Based on Cantor's theorem [46], coefficients of the cosine series in Eq. (26) equal zero. Applying Eq. (24), it arrives

$$\frac{k}{E_1 A_1} h\alpha_m A_m + \frac{2\left[(-1)^m u_1'(L) - u_1'(0)\right]}{L} - \left(\alpha_m^2 + \frac{k}{EA}\right) B_m = 0 \tag{27}$$

in which $\frac{1}{EA} = \frac{1}{E_1 A_1} + \frac{1}{E_2 A_2}$ . Further simplification can be made by substituting the boundary conditions of Eq. (14c), which results in

$$\frac{k}{E_1 A_1} h\alpha_m A_m + 2\sum_{i=1}^{M} D_{\mathrm{im}} \alpha_i^2 B_i - \left(\alpha_m^2 + \frac{k}{EA}\right) B_m = 0 \tag{28}$$

The derivation of $D_{\mathrm{im}}$ is shown in 6.

At last, the fourth derivative of $w$ and the third derivative of $u_1$ are given by

$$w''''(x) = -\sum_{m=1}^{\infty} \alpha_m \left\{ \frac{2}{L}\left[(-1)^m w''(L) - w''(0)\right] - \alpha_m^3 A_m \right\} \sin \alpha_m x \tag{29}$$

$$u_1'''(x) = -\sum_{m=1}^{\infty} \alpha_m \left\{ \frac{2}{L}\left[(-1)^m u_1'(L) - u_1'(0)\right] - \alpha_m^2 B_m \right\} \sin \alpha_m x \tag{30}$$

in which $0 < x < L$. After substituting the load function of Eq. (18) and displacement derivatives of Eqs. (29) and (30) in Eq. (11), the first governing equation can be expressed as:

$$\begin{aligned} &\sum_{m=1}^{\infty} \left\{ -EI_o \alpha_m \frac{2}{L}\left[(-1)^m w''(L) - w''(0)\right] - E_1 A_1 h\alpha_m \frac{2}{L}\left[(-1)^m u_1'(L) - u_1'(0)\right] \right. \\ &\left. + EI_o \alpha_m^4 A_m + E_1 A_1 h\alpha_m^3 B_m - Q_m \right\} \sin \alpha_m x = 0 \end{aligned} \tag{31}$$

Based on Cantor's theorem [46], coefficients of the trigonometric series in Eq. (31) equal zero, which arrives

$$\begin{aligned} &- EI_o\alpha_m \frac{2}{L}\left[(-1)^m w''(L) - w''(0)\right] - E_1A_1h\alpha_m \frac{2}{L}\left[(-1)^m u_1'(L) - u_1'(0)\right] \\ &+ EI_o\alpha_m^4 A_m + E_1A_1h\alpha_m^3 B_m = Q_m \end{aligned} \tag{32}$$

Applying Eq. (14b), Eq. (32) can be rearranged as:

$$\alpha_m \frac{2}{L}\left[(-1)^m R_{\mathrm{L}} w'(L) + R_0 w'(0)\right] + EI_o\alpha_m^4 A_m + E_1A_1h\alpha_m^3 B_m = Q_m \tag{33}$$

Using Eq. (20), it can be obtained that

$$w'(L) = \sum_{m=1}^{\infty}(-1)^m \alpha_m A_m, \quad w'(0) = \sum_{m=1}^{\infty} \alpha_m A_m \tag{34}$$

Substituting Eq. (34) into Eq. (33), it gives

$$EI_o\alpha_m^4 A_m + \frac{2}{L}\alpha_m \sum_{i=1}^{\infty}\left[(-1)^{i+m} R_{\mathrm{L}} + R_0\right]\alpha_i A_i + E_1A_1h\alpha_m^3 B_m = Q_m \tag{35}$$

For convenience, a non-dimensional parameter, $r$, was introduced herein to replace the rotational restraint stiffness, $R$, as

$$r = \frac{1}{1 + \frac{3EI_o}{RL}} \tag{36}$$

in which $r$ is so-called end fixity factors, which is widely used in semi-rigid steel frame connections [38,47]. In particular, $r = 0$ represents the simply supported condition and $r = 1$ is used for the fully clamped. Accordingly, Eq. (35) can be expressed as:

$$EI_o\alpha_m^4 A_m + \frac{6EI_o\alpha_m}{L^2} \sum_{i=1}^{\infty}\left[(-1)^{i+m}\frac{r_{\mathrm{L}}}{1 - r_{\mathrm{L}}} + \frac{r_0}{1 - r_0}\right]\alpha_i A_i + E_1A_1h\alpha_m^3 B_m = Q_m \tag{37}$$

Equations (28) and (37) are two infinite systems of linear equations with respect to coefficients $A_m$ and $B_m$. (Here, the subscripts were set as the same for convenience.) The infinite number of equations can be truncated to finite terms, say $M$, for each coefficients. (The truncated terms for $A_m$ and $B_m$ can be different as well.) Then, it will produce $2M$ equations with $2M$ unknown coefficients, which can be easily solved. Once coefficients $B_m$ have been determined, $C_m$ can also be calculated based on Eq. (24). As a result, all exact displacements, $w(x)$, $u_1(x)$ and $u_2(x)$, can be determined. In addition, the slip can be obtained by using Eq. (1). With all these displacements known, other moments and inner forces can easily be derived, which are not presented here.

The results are theoretically exact when the number of terms is infinite. Convergent solutions with sufficient accuracy can be obtained by a finite number of terms. The larger the number of terms used in a particular analysis, the more accurate the solution will be. No generalizations can be made concerning the choice of an adequate number of terms, as this will vary depending upon the load distribution and boundary restraints. Zhang and Xu [38] have shown that this type of solution converges rapidly for orthotropic plates with rotationally restrained edges. A similar fast convergence can also be observed for the composite beam in this study. For all results presented in this study, $M$ is taken to be 1000.

## 4 Validations with other models

In this section, the proposed series-type solution was validated and compared with other existing composite beam models by considering specific supporting conditions and loading patterns.

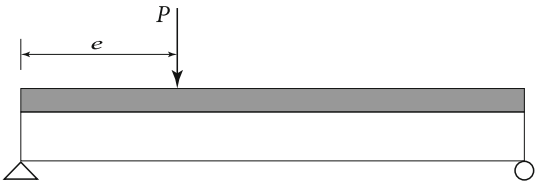


**Fig. 6** Concentrated load located $e$ from left-hand support

### 4.1 Reduce to the simply supported condition

The preceding sections are devoted to composite beams with general boundary conditions which include simply supported and fully clamped as well as their intermediate cases. Such general expressions can be reduced to the simply supported case by assuming zero rotational ($R_0 = R_L = 0$) and end-slip ($K_0 = K_L = 0$) restraints in Eqs. (35) and (28). Then, Eqs. (35) and (28) can be reduced to the following form:

$$EI_o\alpha_m^4 A_m + E_1A_1h\alpha_m^3 B_m = Q_m \tag{38a}$$

$$\frac{kh}{E_1A_1}\alpha_m A_m - \left(\alpha_m^2 + \frac{k}{EA}\right) B_m = 0 \tag{38b}$$

Fourier coefficients $A_m$ and $B_m$ can easily be solved from the above set of equations. Then, the exact displacement of composite beam under arbitrary transverse loads is given by

$$w(x) = \sum_{m=1}^{\infty} \frac{1}{EI_o + \frac{kh^2}{\alpha_m^2 + k/EA}} \frac{Q_m}{\alpha_m^4} \sin\alpha_m x \tag{39}$$

The value of constant $Q_m$ in Eq. (39) was defined in Eq. (19), which is dependent upon the type of load distribution. The most common types of load distribution are uniform distributed loads and concentrated loads. For a uniform distributed load, $q$, along the span,

$$Q_m = \frac{2q}{m\pi}(1 - (-1)^m) \tag{40}$$

For a concentrated load, $P$, as shown in Fig. 6

$$Q_m = \frac{2P}{L}\sin\alpha_m e \tag{41}$$

where $e$ is the distance of the load from left-hand support.

Smith [30] derived exact series-type solutions for deflections of built-up composite beams by expressing the moment and sectional normal forces due to applied load as two Fourier series. The present solution in Eq. (39) is equivalent to those results by Smith [30] but in a more concise form.

### 4.2 Deduction of Gamma method

Van der Linden [20] presented a closed-form solution for a simply supported composite beam with a sinusoidal load along its length and deduced equivalent expressions of the Gamma method, which can also be derived by the present series-type solution. The sinusoidal load can be defined as:

$$q(x) = q_0 \sin\alpha_1 x \tag{42}$$

where $\alpha_1 = \pi/L$, which is the value of $\alpha_m$ in Eq. (18) when $m = 1$. In this manner, the displacement function can be also expressed in a sinusoidal shape as:

$$w(x) = A \sin\alpha_1 x \tag{43}$$

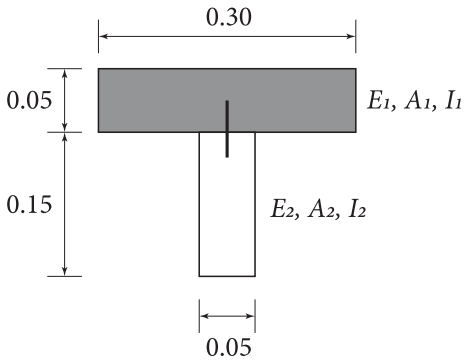


**Fig. 7** A single span timber–concrete beam (unit: meter; the upper element is denoted as element 1 and the lower element is element 2)

From Eq. (39), the constant $A$ can be derived as:

$$A = \frac{q_0 L^4}{\pi^4 E I_{\text{eff}}} \tag{44}$$

in which $EI_{\text{eff}}$ is the effective flexural stiffness and is expressed as:

$$EI_{\text{eff}} = EI_o + \frac{kh^2}{\left(\frac{\pi}{L}\right)^2 + \frac{k}{EA}} \tag{45}$$

Equations (45) differ from the way Van der Linden presented in [20], and the results are nevertheless the same. Further rearrangements can be carried out leading to the prominent expression of Gamma method proposed in the Annex B of the Eurocode 5 [17]

$$EI_{\text{eff}} = EI_o + \gamma E_1 A_1 (h-a)^2 + E_2 A_2 a^2 \tag{46}$$

in which $\gamma = [1 + \pi^2 E_1 A_1/(kL^2)]^{-1}$ is the shear connection reduction factor and $a$ is the distance from the centroid of the bottom element to the neutral axis of the composite section, which is given by

$$a = \frac{\gamma E_1 A_1}{\gamma E_1 A_1 + E_2 A_2} h \tag{47}$$

## 5 Numerical examples and parametric studies

In this section, a 4 m single-span timber–concrete composite beam reported by Girhammer in [16] was studied. The cross section and dimensions of the beam are shown in Fig. 7. The material properties are $E_1 = 12$ GPa and $E_2 = 8$ GPa. The slip modulus (i.e. stiffness of shear connectors) is $k = 50$ N/mm/mm. For this beam, the influence of end slip restraints was first discussed, followed by deflection predictions and comparisons with other models.

### 5.1 Influence of end slip restraints

Based on the expression of $D_{\text{im}}$ in Eq. (A.6), a non-dimensional parameter, $\lambda$, was defined herein for end-slip restraints as:

$$\lambda_0 = \frac{K_0}{kL}, \quad \lambda_{\text{L}} = \frac{K_{\text{L}}}{kL} \tag{48}$$

where $k$ is the slip modulus, $K_0$ and $K_{\text{L}}$ are stiffness of end-slip restraints at two ends, respectively, and the associated parameters are $\lambda_0$ and $\lambda_{\text{L}}$. For simplicity, $\lambda_0 = \lambda_{\text{L}} = \lambda$ in the following analysis. $\lambda$ represents the relative importance of the end-slip restraints compared to the shear connectors. A very large variation in $\lambda$ is

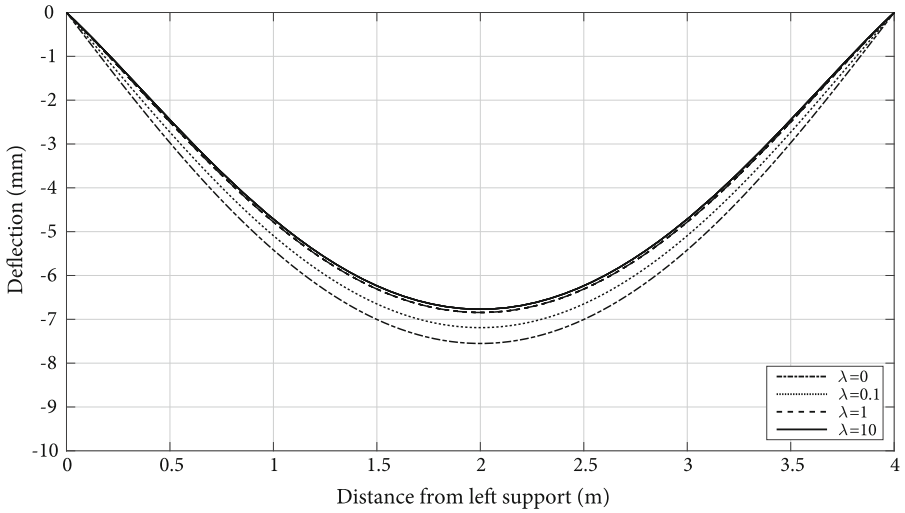


**(a)** Deflection

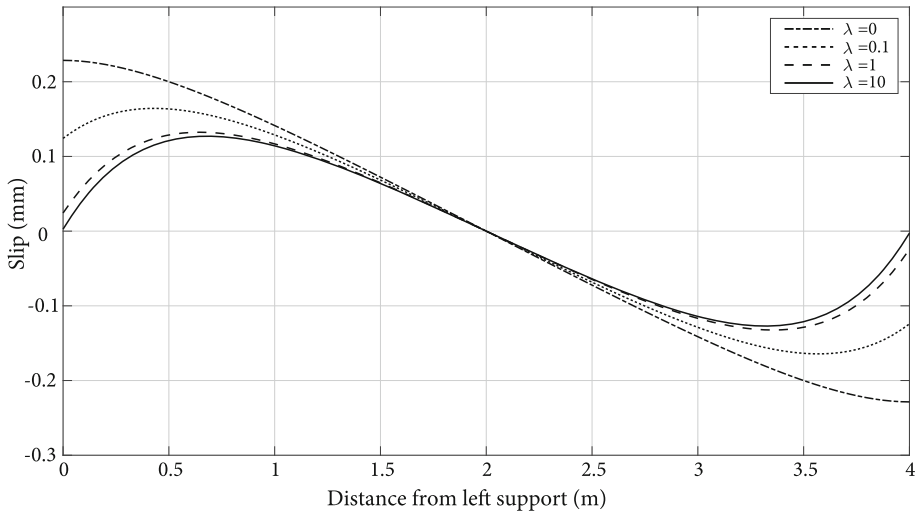


**(b)** Slip

**Fig. 8** Deflections and slips of a simply supported composite beam with various end-slip restraints under a distributed load

possible: λ equal to zero corresponds to no end-slip restraints, and a higher λ results in smaller slip at beam ends.

First, consider the beam in Fig. 7 simply supported and loaded by a uniformly distributed load, 1 kN/m. For this beam, four different end-slip restraints were studied and the associated values of λ were 0, 0.1, 1 and 10. The beam displacements and slips were determined for the four cases as illustrated in Fig. 8. It can be found that both displacements and slips were notably affected by the end-slip restraints. More importantly, the slips at beam ends were close to zero when $\lambda \geqslant 1$, extremely close for $\lambda = 10$, as shown in Fig. 8b. Thus, it can be imagined that when the non-dimensional end-slip parameter λ is larger than 10, the relative slip at beam ends can be considered to be fully suppressed and the slip at other beam positions will almost be the same for different λ.

Similarly, parametric studies were conducted for the same simply supported composite beam with different slip moduli. Four slip moduli were considered, namely $k = 1$, 5, 25 and $50\,N/mm/mm$. For each slip modulus, two end-slip restraint scenarios were investigated: $\lambda = 0$ and $\lambda = 1$. In order to illustrate the influence of end-slip restraints varying with different slip moduli, both numerical results of two different λ were presented in the

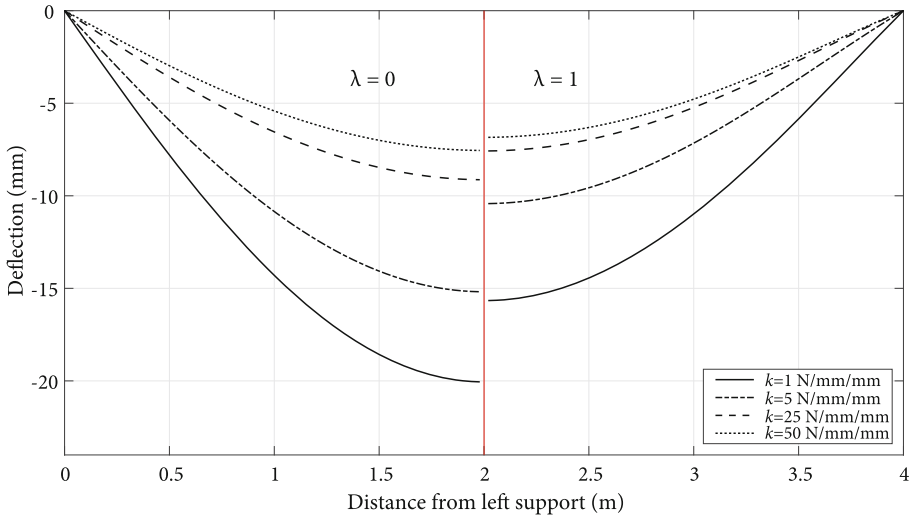


**(a)** Deflection (left hand side: $\lambda = 0$ and right hand side: $\lambda = 1$)

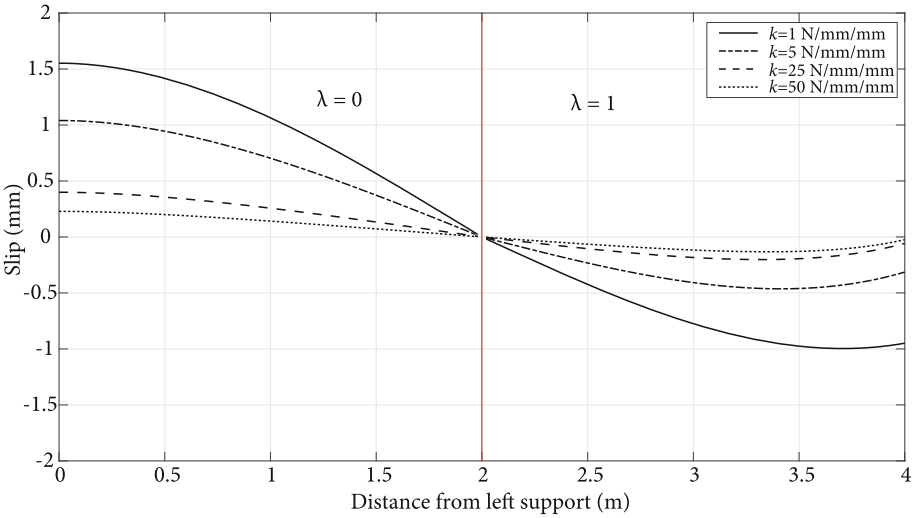


**(b)** Slip (left hand side: $\lambda = 0$ and right hand side: $\lambda = 1$)

**Fig. 9** Deflections and slips of a simply supported composite beam with various slip moduli

same figure (left-hand side is for $\lambda = 0$ and right hand side $\lambda = 1$). In this manner, Fig. 9 demonstrates the beam displacements and slips for the composite beam with different slip moduli and end-slip restraints. It is clear that the effect of end-slip restraints is more evident in the case with smaller slip moduli (see $k = 1$ N/mm/mm).

**Table 1** Maximum deflection of a single-span composite beam

| Boundary conditions | Load distributions | Maximum deflections (mm) | | |
|---|---|---|---|---|
| | | Girhammar [16] | Present | Difference (%) |
| Pinned-pinned | Distributed load (1 kN/m) | 7.56 | 7.526 | −0.4 |
| | Point load (1 kN) | 3.08 | 3.061 | −0.6 |
| Pinned-clamped | Distributed load (1 kN/m) | 4.01 | 3.995 | −0.4 |
| | Point load (1 kN) | 1.76 | 1.754 | −0.3 |
| Clamped-clamped | Distributed load (1 kN/m) | 2.32 | 2.323 | 0.1 |
| | Point load (1 kN) | 1.16 | 1.159 | −0.1 |

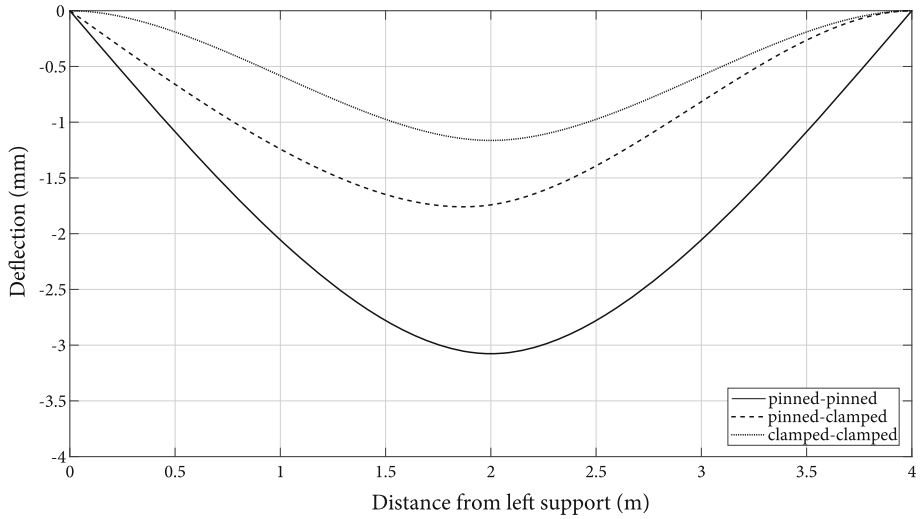


**(a)** Deflection

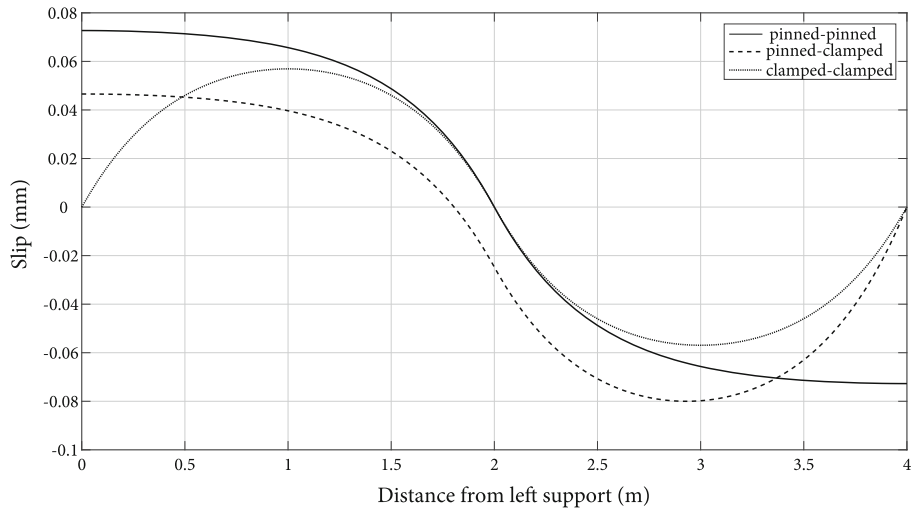


**(b)** Slip

**Fig. 10** Deflections and slips of a composite beam with various end support conditions under a concentrated load

## 5.2 Influence of end support restraints

Not only the simply supported boundary (pinned-pinned) conditions, but also pinned–clamped and clamped–clamped conditions were analysed and compared with results reported in [16]. For the simply supported case, $r$ and $\lambda$ were both set as zero. The clamped cases were simulated by setting $r = 0.999$ [$r = 1$ results in a zero denominator in Eq. (37)] and $\lambda = 10{,}000$ (far enough for end-slip restraints). Two transverse loading scenarios were examined: uniformly distributed loading and mid-span concentrated loading. The results and comparisons are presented in Table 1. It can be seen that the present results obtained from exact series solutions are in excellent agreement with results in [16]. In addition, the displacement and slip curves for the concentrated loading case are presented in Fig. 10.

Since very little results can be found for composite beams with rotational restrained edges, no comparison was conducted for those restrained cases. For demonstration, the displacements and slips of restrained composite beams ($r = 0.5$) with different end-slip restraints ($\lambda = 0, 0.1$ & $1$) are presented in Fig. 11 as well as the simply supported case ($r = 0$ & $\lambda = 0$) and the clamped case ($r = 0.999$ & $\lambda = 10{,}000$). It can be

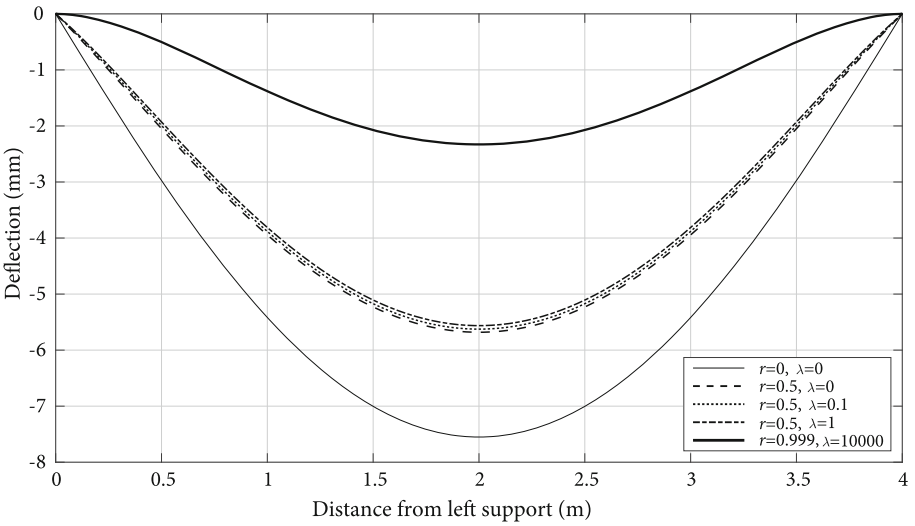


**(a)** Deflection

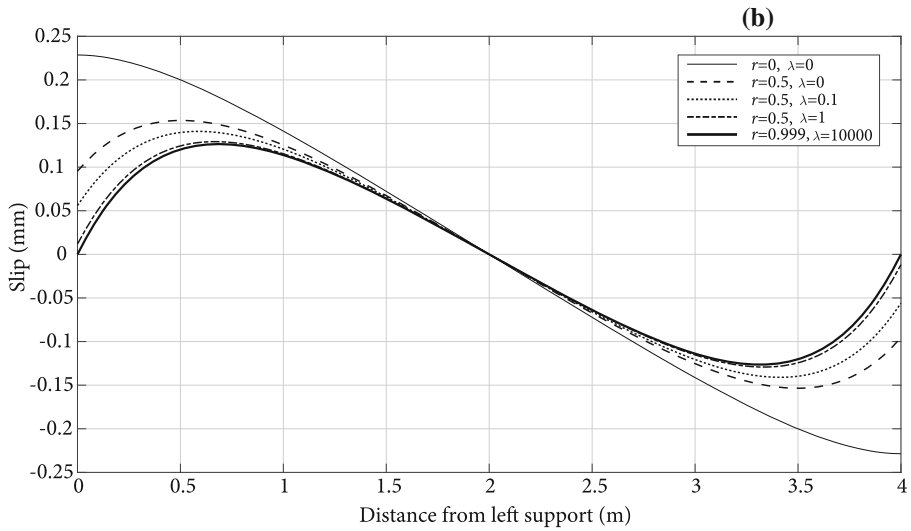


**(b)** Slip

**Fig. 11** Deflections and slips of a composite beam with various end support conditions under a distributed load

observed that the deflection and slip of composite beams are highly dependent on boundary restraints. More importantly, the end-slip restraints have a marginal influence on the deflection but a major effect on the slip.

## 6 Conclusions

The behaviour of composite beams is governed by load distributions and actual boundary conditions. Existing solutions normally deal with classical boundary conditions, namely free, simply supported and clamped, which often deviates from the actual conditions in reality. The realistic supporting conditions are generally semi-rigid, especially for timber structures since it is notoriously difficult to achieve fully clamped conditions for timber elements. The current study first summarized widely used design methods for composite beams both in Europe and North America, and concluded that they are basically the same method. Then, an analytical model for composite beams with rotationally restrained edges was developed, and its exact series solutions were derived by using Stokes' transformation.

By comparing them to other simple models, it has been shown that the recently proposed model can be reduced to the simple models by setting the end restraints to zero. The parametric studies revealed that both rotational and end-slip restraints significantly influence the deflection and interlayer slip of composite beams. Particularly, the effect of end-slip restraints is more evident when the slip modulus is small, and is notable for slips but marginal for deflections.

In the future, the proposed model can be useful as a benchmark for future analysis such as finite-element modelling. Simple design formulas can also be developed for hand-calculation design solutions.



**Declarations**

**Conflict of interests** The authors declared no potential conflicts of interest with respect to the research, authorship and/or publication of this article.

## Appendix A: Derivation of $D_{\text{im}}$

By using Eqs. (14c) and (25), $u_1'(0)$ and $u_1'(L)$ can be expressed as:

$$u_1'(0) = \frac{K_0}{kL}\left[u_1'(L) - u_1'(0)\right] + \frac{K_0}{k}\sum_{m=1}^{\infty}\left\{\frac{2}{L}\left[(-1)^m u_1'(L) - u_1'(0)\right] - \alpha_m^2 B_m\right\} \tag{A.1}$$

$$u_1'(L) = -\frac{K_{\text{L}}}{kL}\left[u_1'(L) - u_1'(0)\right] - \frac{K_{\text{L}}}{k}\sum_{m=1}^{\infty}\left\{\frac{2}{L}\left[u_1'(L) - (-1)^m u_1'(0)\right] - (-1)^m \alpha_m^2 B_m\right\} \tag{A.2}$$

For numerical calculations, the sum of infinite terms in Eqs. (A.1) and (A.2) can be approximately evaluated by the partial sum of finite terms by truncating the infinite number of terms to finite terms, $M$. Then, a system of functions about $u_1'(0)$ and $u_1'(L)$ can be derived by rearranging Eqs. (A.1) and (A.2).

$$\left[1 + (2M+1)\frac{K_0}{kL}\right]u_1'(0) - (-1)^M \frac{K_0}{kL}u_1'(L) = -\frac{K_0}{k}\sum_{m=1}^{M}\alpha_m^2 B_m \tag{A.3a}$$

$$(-1)^M \frac{K_{\text{L}}}{kL}u_1'(0) - \left[1 + (2M+1)\frac{K_{\text{L}}}{kL}\right]u_1'(L) = -\frac{K_{\text{L}}}{k}\sum_{m=1}^{M}(-1)^m \alpha_m^2 B_m \tag{A.3b}$$

$u_1'(0)$ and $u_1'(L)$ can readily be solved and $(-1)^m u_1'(L) - u_1'(0)$ can be expressed as:

$$\frac{(-1)^m u_1'(L) - u_1'(0)}{L} = \sum_{i=1}^{M}\left\{(-1)^i \frac{(-1)^m A - B}{AD - BC}\frac{K_{\text{L}}}{kL} - \frac{(-1)^m C - D}{AD - BC}\frac{K_0}{kL}\right\}\alpha_i^2 B_i \tag{A.4}$$

in which

$$A = 1 + (2M+1)\frac{K_0}{kL}, \quad B = (-1)^M \frac{K_0}{kL} \tag{A.5a}$$

$$C = (-1)^M \frac{K_{\text{L}}}{kL}, \quad D = 1 + (2M+1)\frac{K_{\text{L}}}{kL} \tag{A.5b}$$

At last, $D_{\text{im}}$ is defined as:

$$D_{\text{im}} = (-1)^i \frac{(-1)^m A - B}{AD - BC}\frac{K_{\text{L}}}{kL} - \frac{(-1)^m C - D}{AD - BC}\frac{K_0}{kL} \tag{A.6}$$

## References


1. Wang, Y.C.: Deflection of steel–concrete composite beams with partial shear interaction. J. Struct. Eng. **124**(10), 1159–1165 (1998)
2. Oehlers, D.J., Bradford, M.A.: Elementary Behaviour of Composite Steel and Concrete Structural Members. Butterworth-Heinemann, Oxford (1999)
3. Johnson, R.P.: Composite Structures of Steel and Concrete: Beams, Slabs, Columns and Frames for Buildings, 3rd edn. Blackwell Publishing, Hoboken (2004)
4. Ceccotti, A.: Composite concrete–timber structures. Prog. Struct. Mat. Eng. **4**(3), 264–275 (2002)
5. Yeoh, D., Fragiacomo, M., De Franceschi, M., Heng Boon, K.: State of the art on timber–concrete composite structures: literature review. J. Struct. Eng. **137**(10), 1085–1095 (2011)
6. Girhammar, U.A., Pan, D.H.: Exact static analysis of partially composite beams and beam–columns. Int. J. Mech. Sci. **49**(2), 239–255 (2007)
7. Stüssi, F.: Zusammengesetzte vollwandträger. Int. Assoc. Bridge Struct. Eng. (IABSE) **8**, 249–269 (1947)
8. Newmark, N.M., Siess, C.P., Viest, I.M.: Tests and analysis of composite beams with incomplete interaction. Proc. Soc. Exp. Stress Anal. **9**(1), 75–92 (1951)
9. Möhler, K.: Über das tragverhalten von biegeträgern und druckstäben mit zusammengestezten querschnitten und nachgiebigen verbindungsmitteln. Ph.D. thesis, Technical University of Karlsruhe (1956)
10. Goodman, J.R.: Layered wood systems with interlayer slip. Ph.D. thesis, University of California, Berkeley, Berkeley, CA, USA (1967)
11. Girhammar, U.A., Gopu, V.K.: Composite beam–columns with interlayer slip-exact analysis. J. Struct. Eng. **119**(4), 1265–1282 (1993)
12. Salari, M.R., Spacone, E., Shing, P.B., Frangopol, D.M.: Nonlinear analysis of composite beams with deformable shear connectors. J. Struct. Eng. **124**(10), 1148–1158 (1998)
13. Frangi, A., Fontana, M.: Elasto-plastic model for timber–concrete composite beams with ductile connection. Struct. Eng. Int. **13**(1), 47–57 (2003)
14. Zhang, C., Gauvreau, P.: Timber–concrete composite systems with ductile connections. J. Struct. Eng. **141**(7), 04014179 (2015)
15. Auclair, S.C., Sorelli, L., Salenikovich, A.: Simplified nonlinear model for timber–concrete composite beams. Int. J. Mech. Sci. **117**, 30–42 (2016)
16. Girhammar, U.A.: A simplified analysis method for composite beams with interlayer slip. Int. J. Mech. Sci. **51**(7), 515–530 (2009)
17. EN 1995-1-1: Eurocode 5—Design of Timber Structures. European Committee for Standardization, Bruxelles, Belgium (2004)
18. McCutcheon, W.J.: Method for predicting the stiffness of wood-joist floor systems with partial composite action, FPL 289, Forest Products Laboratory, Forest Service, U.S. Department of Agriculture, Madison, Wisconsin, USA (1977)
19. McCutcheon, W.J.: Stiffness of framing members with partial composite action. J. Struct. Eng. **112**(7), 1623–1637 (1986)
20. van der Linden, M.L.R.: Timber–concrete composite floor systems. HERON **44**(3), 215–239 (1999)
21. Fernandez-Cabo, J.L., Fernandez-Lavandera, J., Diez-Barra, R., Avila-Jalvo, J.M.: Timber composite beams with a discrete connection system. Proc. Inst. Civ. Eng. Struct. Build. **166**(2), 57–72 (2013)
22. Allen, D.E., Onysko, D.M., Murray, T.M.: Minimizing Floor Vibration. ATC Design Guide 1. Applied Technology Council, Redwood City, California (1999)
23. Heimeshoff, B.: Näherungsverfahren zur berechnung von einfeldträgern mit kragarm und von zweifeldträgern, die aus nachgiebig miteinander verbundenen querschnittsteilen bestehen, im ingenieurholzbau. Holz als Roh-und Werkstoff **49**(7), 277–285 (1991)
24. Xu, R., Chen, D.: Variational principles of partial-interaction composite beams. J. Eng. Mech. **138**(5), 542–551 (2012)
25. Atashipour, S.R., Landel, P., Al-Emrani, M.: Accuracy evaluation of gamma-method for deflection prediction of partial composite beams. In: 2018 World Conference on Timber Engineering (WCTE 2018), Seoul, Republic of Korea (2018)
26. Koiter, W.T.: Discussion: "Timoshenko beam theory is not always more accurate than elementary beam theory". J. Appl. Mech. **44**(2), 357–358 (1977)
27. Chui, Y., Smith, I.: Influence of rotatory inertia, shear deformation and support condition on natural frequencies of wooden beams. Wood Sci. Technol. **24**(3), 233–245 (1990)
28. Zhang, S., Zhou, J., Niederwestberg, J., Chui, Y.H.: Effect of end support restraints on vibration performance of cross laminated timber floors: an analytical approach. Eng. Struct. **189**, 186–194 (2019)
29. Timoshenko, S., Woinowsky-Krieger, S.: Theory of Plates and Shells, 2nd edn. McGraw-Hill, Inc., New York (1959)
30. Smith, I.: Series type solutions for built-up timber beams with semi-rigid connections. Proc. Inst. Civ. Eng. **69**(3), 707–719 (1980)
31. Amana, E.J., Booth, L.G.: Theoretical and experimental studies on nailed and glued plywood stressed-skin components, Part I. Theoretical study. J. Inst. Wood Sci. **4**(1), 43–69 (1967)
32. Zhang, S., Xu, L.: Exact static analysis of eccentrically stiffened plates with partial composite action. Compos. Struct. **198**, 117–125 (2018)
33. Gorman, D.J.: Vibration Analysis of Plates by the Superposition Method. Series on Stability, Vibration and Control of Systems, Series A, vol. 3. World Scientific, Singapore (1999)
34. Bhaskar, K., Kaushik, B.: Simple and exact series solutions for flexure of orthotropic rectangular plates with any combination of clamped and simply supported edges. Compos. Struct. **63**(1), 63–68 (2004)
35. Greif, R., Mittendorf, S.: Structural vibrations and Fourier series. J. Sound Vib. **48**(1), 113–122 (1976)
36. Wang, J.T.-S., Lin, C.-C.: Dynamic analysis of generally supported beams using Fourier series. J. Sound Vib. **196**(3), 285–293 (1996)

37. Li, R., Zhong, Y., Tian, B., Liu, Y.: On the finite integral transform method for exact bending solutions of fully clamped orthotropic rectangular thin plates. Appl. Math. Lett. **22**(12), 1821–1827 (2009)
38. Zhang, S., Xu, L.: Bending of rectangular orthotropic thin plates with rotationally restrained edges: a finite integral transform solution. Appl. Math. Model. **46**, 48–62 (2017)
39. Wu, Y.-F., Xu, R., Chen, W.: Free vibrations of the partial-interaction composite members with axial force. J. Sound Vib. **299**(4), 1074–1093 (2007)
40. Gjelsvik, A.: Analog-beam method for determining shear-lag effects. J. Eng. Mech. **117**(7), 1575–1594 (1991)
41. Betti, R., Gjelsvik, A.: Elastic composite beams. Comput. Struct. **59**(3), 437–451 (1996)
42. Ellakany, A.M., Tablia, H.A.: A numerical model for static and free vibration analysis of elastic composite beams with end shear restraint. Meccanica **45**(4), 463–474 (2010)
43. Tolstov, G.P.: Fourier Series. Dover Publications, New York (1962)
44. Bromwich, T.J.I.: An Introduction to the Theory of Infinite Series, 2nd edn. Macmillan and Company, New York (1965)
45. Zhang, S.: Vibration serviceability of cold-formed steel floor systems. Ph.D. thesis, University of Waterloo, Waterloo, ON, Canada (2017)
46. Bary, N.K.: A Treatise on Trigonometric Series, vol. 1. Pergamon Press Ltd., Oxford (1964)
47. Xu, L.: Second-order analysis for semirigid steel frame design. Can. J. Civ. Eng. **28**(1), 59–76 (2001)